

UC Davis

UC Davis Previously Published Works

Title

Novel sorafenib-based structural analogues

Permalink

<https://escholarship.org/uc/item/11t1c300>

Journal

Anti-Cancer Drugs, 25(4)

ISSN

0959-4973

Authors

Wecksler, Aaron T

Hwang, Sung Hee

Wettersten, Hiromi I

et al.

Publication Date

2014-04-01

DOI

10.1097/cad.0000000000000079

Peer reviewed



Published in final edited form as:

Anticancer Drugs. 2014 April ; 25(4): 433–446. doi:10.1097/CAD.0000000000000079.

Novel Sorafenib-Based Structural Analogues: In Vitro Anticancer Evaluation of *t*-MTUCB and *t*-AUCMB

Aaron T. Wecksler^{a,b}, Sung Hee Hwang^{a,b}, Hiromi I. Wettersten^c, Jennifer E. Gilda^d, Amy Patton^d, Leonardo J. Leon^{b,e}, Kermit L. Carraway III^{b,e}, Aldrin V. Gomes^d, Keith Baar^d, Robert H. Weiss^{b,c,f}, and Bruce D. Hammock^{a,b,*}

^aDepartment of Entomology and Nematology, University of California Davis, One Shields Avenue, Davis, CA, USA 95616

^bUC Davis Comprehensive Cancer Center, Sacramento, CA, USA 95817

^cDepartment of Internal Medicine, Division of Nephrology, University of California, Davis Medical Center, Sacramento, CA, USA 95817

^dDepartment of Neurobiology, Physiology and Behavior, University of California Davis, Davis, CA, USA 95616

^eDepartment of Biochemistry and Molecular Medicine, University of California Davis School of Medicine, Sacramento, CA, USA 95817

^fU.S. Department of Veterans' Affairs Medical Center, Sacramento, CA, USA 95655

Abstract

In the current study, we performed a mechanistic study on the cytotoxicity of two compounds, *t*-AUCMB and *t*-MTUCB, that are structurally similar to sorafenib. These compounds display strong cytotoxic responses in various cancer cell lines, despite significant differences in the induction of apoptotic events such as caspase activation and lactate dehydrogenase release in hepatoma cells. Both compounds induce autophagosome formation and LC3I cleavage, but there was little observable effect on mTORC1 or the downstream targets, S6K1 and 4E-BP1. In addition, there was an increase in activity of upstream signaling through the IRS1/PI3K/Akt signaling pathway, suggesting that unlike sorafenib, both compounds induce mTOR-independent autophagy. The observed autophagy correlates with mitochondrial membrane depolarization, AIF release, and oxidative stress-induced glutathione depletion. However, there were no observable changes in the ER-stress markers such as Bip, IRE α , p-eIP2, and the lipid peroxidation marker, 4-HNE, suggesting ER-independent oxidative stress. Finally, these compounds do not possess the multikinase inhibitory activity of sorafenib, which may be reflected in their difference in ability to halt cell cycle progression compared to sorafenib. Our findings indicate that both compounds have anti-cancer effects comparable to sorafenib in multiple cell line, but they induce significant differences in apoptotic responses and appear to induce mTOR-independent autophagy. *t*-AUCMB and *t*-MTUCB, represent novel chemical probes that are capable of inducing mTOR-independent autophagy and apoptosis to differing degrees, and thus may be potential tools for further understanding the link between these two cellular stress responses.

*Corresponding author. Tel: 530-752-7519 (office). Fax: 530-752-1537. bdhammock@ucdavis.edu.

Conflict of Interest

None declared.

Keywords

Sorafenib; sorafenib analogues; hepatoma cells; autophagy; oxidative stress; kinase selectivity profiling

Introduction

Sorafenib (Nexavar[®]), a novel multikinase inhibitor, is the only FDA-approved small molecule drug to treat hepatocellular carcinoma (HCC). Our laboratory has found that sorafenib is also a potent inhibitor of soluble epoxide hydrolase (sEH) [1], leading to the synthesis of a series of compounds that are structurally similar to sorafenib but possess various kinase inhibitory selectivity [2]. Among them we identified two compounds, *t*-AUCMB and *t*-MTUCB, possessing comparable cytotoxicity to sorafenib, but without inhibitory activity against the primary targets of sorafenib, such as C-Raf kinase and vascular endothelial growth factor receptor 2 (VEGFR2) kinase. Thus, we were interested in understanding the nature of this observed cytotoxicity and the effect of these compounds on cell death.

Resistance to sorafenib has recently been attributed to its broad spectrum kinase inhibition and the induction of mammalian target of rapamycin (mTOR)-dependent autophagy [3]. Traditionally, mechanisms leading to autophagy have been separated into two distinct categories: mTOR-dependent autophagy and mTOR-independent autophagy. mTOR-dependent autophagy combines both extracellular and intracellular signaling through the mTORC1 complex, suppressing the induction of autophagy when activated [4]. Key members of this pathway include the PI3K/PDK/Akt signaling cassette upstream and the downstream phosphorylation targets eukaryotic initiation factor 4E binding protein (4EBP1) and S6K1. Sorafenib was shown to induce mTOR-independent autophagy through the inhibition of PI3K and S6K1 [3]. mTOR-independent autophagy is less well understood and can result from a variety of stimuli including, calcium flux [5], reduced cellular ATP (sensed via AMPK) [6], mitochondrial depolarization (mitophagy) [7], oxidative stress [8], and proteasome inhibition [9]. Many studies on the role of autophagy in cancer suggest this process may contribute to tumor cell survival and chemotherapeutic resistance [10], as proposed for sorafenib. Thus, studies involving anticancer drugs with structural similarities to sorafenib require investigating both cytotoxic and autophagic responses.

The current work examines the kinase inhibitory profile of *t*-AUCMB and *t*-MTUCB, and evaluates their cytotoxicity across various cancer cell lines. Extensive characterization was performed to compare their cellular responses to sorafenib in hepatoma cell lines, including caspase-dependent and caspase-independent apoptosis, effects on cell cycle progression, mitochondrial depolarization and apoptosis-inducing factor (AIF) release, induction of autophagy, endoplasmic reticulum (ER)-related oxidative stress, and effect on the ubiquitin-proteasome system. This work demonstrates that despite similar overall observed cytotoxicity, the distinct structural features of *t*-AUCMB and *t*-MTUCB confer unique mechanisms of cell death in hepatoma cells.

Materials and Methods

Compounds

Sorafenib and bortezomib were purchased from LC Laboratories. Oleuropein was purchased from Sigma-Aldrich (Woburn, MA). MG132 was purchased from EMD Millipore (Billerica, Massachusetts). All other compounds were synthesized as previously described [2].

Cell Lines

The HepG2 human cell line was obtained from American Type Culture Collection (ATCC, Rockville, MD). The Huh-7 human cell line was provided by Dr. Jian Wu, University of California Davis Medical Center, Sacramento, CA. The PC-3 cell line was provided by Professor Maria Mudryj, University of California Davis, Davis, CA. The HepG2, Huh-7 and PC-3 cell lines were cultured in Eagle's Minimum Essential Medium containing 10% fetal bovine serum (FBS) and 1% penicillin-streptomycin. The T47D (Dulbecco's Modified Eagles Medium containing 15% fetal bovine serum (FBS) and 1% penicillin-streptomycin) and SKBR3 (RMPI with 10% FBS, 10 mM HEPES, 1 mM Sodium Pyruvate, 14 mM glucose, 1 mg/ml insulin, and 1% penicillin-streptomycin) cell lines were provided by Professor Colleen Sweeney, University of California Davis Comprehensive Cancer Center, Sacramento, CA. All cell lines were incubated in 5% CO₂ at 37 °C.

Cell Viability, Lactate Dehydrogenase Release, and Caspase-Induction

Cells were plated at 10,000 cells per well in 96-well plates and allowed to attach overnight under the growth conditions described above. On the following day, sorafenib or the synthetic analogues were added to each well and incubated for the length of time indicated. These compounds were dissolved in DMSO and diluted with Eagle's Minimal Essential Medium to the desired concentration of 0.1 μM, 1.0 μM, 5.0 μM, 10 μM, and 25 μM, with a final DMSO concentration of 0.1% for all cell-based *in vitro* studies. Cell viability was determined using the 3-(4,5-dimethylthiazol-2-yl)-2,5-diphenyltetrazolium bromide (MTT) Cell Viability Assay Kit according to manufacturer's instructions (ATCC, Rockville, MD). The 96-well plates were measured at 570 nm using SpectroMax 190 plate reader (Molecular Devices). The effective concentrations (EC₅₀) at which the cell viability is 50% as compared to the DMSO control was calculated using nonlinear regression analysis with the KaleidaGraph graphing program (Synergy Software). The lactate dehydrogenase (LDH) cytotoxicity detection kit (Clontech, Mountain View, CA) was used as a marker of plasma membrane depolarization. Measurement of LDH activity was determined by measuring the absorbance at 490 nm using SpectroMax 190 plate reader (Molecular Devices) and the percent cytotoxicity was determined as described by the manufacturer. Caspase 3/7 activation was determined using Caspase-Glo 3/7 Assay (Promega, Madison, WI) and luminescent readings were performed using a SpectroFluor Plus luminescence plate reader (Tecan). All data were plotted as difference between the DMSO control luminescence (RLU) and the total luminescence (RLU) from each concentration of compound. Each concentration was performed in triplicate per 96-well plate and EC₅₀ data are presented as the mean ± standard deviation from at least three separate experiments performed on separate days.

Apoptosis-Inducing Factor Imaging and Autophagy Detection

Caspase-independent programmed cell death responses were determined by analyzing the mitochondrial membrane depolarization and nuclear translocation of apoptosis-inducing factor (AIF). HepG2 cells were seeded at 200,000 cells/well in 12-well plates containing an 18 mm glass coverslip. Cells were allowed to attach overnight then incubated with various compounds at 30 μM concentration for six hours. Mitochondrial staining was performed by incubating cells with MitoTracker[®] Red CMXRos (Invitrogen, Carlsbad, CA) for 15 minutes. Cells were then rinsed with PBS and fixed in 4% paraformaldehyde/PBS solution for 15 minutes. Fixed cells were permeabilized using 0.2% Triton X-100/PBS for 5 min, washed and then incubated with primary rabbit antibody against AIF (Cell Signaling Technology Inc., Beverly, MA) for 1 hour. Cells were then treated with anti-rabbit Alexa Fluor[®] 488 secondary antibody (Cell Signaling Technology Inc.) and incubated for an additional hour. Samples were then washed and placed cell-side down onto a drop of DAPI-

containing mounting solution (Vector Laboratories, Burlingame, CA) on a glass slide and dried for 30 minutes. Confocal fluorescence microscopy was carried out with an Olympus FV1000 laser point microscope, and the images were analyzed using Olympus FLUOVIEW (FV10-ASW) Software Package. Autophagy was detected using the Cyto-ID[®] Autophagy Detection Kit (Enzo Life Sciences, Farmingdale, NY). Cellular assays were performed as described for AIF except that cells were prepared for live-cell imaging. Sample preparation and analysis was performed as described by the manufacturer. Autophagosomal vacuoles were analyzed using a Leica DMI6000 B inverted fluorescence microscope with Differential Interference Contrast (DIC), and data were analyzed using ImageJ software package.

Cell Cycle Analysis

Cell cycle analysis was performed using the Click-it[®] EdU Alexa Fluor[®] 488 Flow Cytometry Assay Kit (Invitrogen, Carlsbad, CA). HepG2 cells were seeded at 1×10^6 cells per well in six-well plates in serum containing medium and allowed to recover for 8 hrs. After 36 hours of synchronization in serum free medium, cell growth was re-initiated with the addition of serum-containing medium for 1 hr in the presence of 10 μ M EdU (5-ethynyl-2'-deoxyuridine). Cells were then incubated with the test compounds at 30 μ M for 24 hours. The cells were fixed and then incubated with the cell cycle dye 7-aminoactinomycin D (7-AAD) for 30 minutes just prior to analysis using a Becton Dickinson FACScan with a Cytex xP5 upgrade. Data acquisition and analysis were performed using BD CellQuest and FlowJo software packages, respectively.

Glutathione Quantification

Quantification of reduced (GSH) and oxidized (GSSG) glutathione was performed as described previously [42]. Briefly, HepG2 cells were plated at 500,000 cells per well in six-well plates (EMEM 10% FBS, 1.0% penicillin-streptomycin) and allowed to recover overnight. The media was then replaced with fresh media containing the desired concentrations of the test compounds at 0.1% DMSO and incubated for 6 hours. Treated cells were washed with PBS buffer and lysed using 200 μ L of binary mobile phase buffer "A" (25 mM NaH₂PO₄ 0.5 mM octane sulfonic acid in water, pH 2.7). Cell lysates were pelleted and 10 μ L of supernatant was loaded onto a Synergi 4 μ Hydro-RP 4.6 \times 250 mm column with a corresponding 2 \times 3 mm guard column (Phenomenex, Torrance, CA). GSH and GSSG were eluted using isocratic flow of 100% "A" for 20 min, then 25% A, 75% "B" (25 mM NaH₂PO₄ 0.5 mM octane sulfonic acid in 10% acetonitrile/H₂O) for 45 minutes, using Waters 510 HPLC solvent delivery system with binary pumps with 717+ Autosampler. Detection was performed using ESA/DIONEX Coulochem II with at 5040 analytical cell (875 mV) and a 520 guard cell (+1400 mV) (Thermo Fisher Scientific) Retention times were approximately 12.5–13.5 and 38–41 minutes for GSH and GSSH, respectively. Glutathione concentrations were expressed as a ratio with respect to total protein concentration.

Proteasome activity assays

The 26S proteasomal assays of the cell lysates were carried out in a total volume of 100 μ L in 96-well plates with 100 μ M ATP in 26S buffer (50 mM Tris, 1 mM EDTA, 150 mM NaCl, 5 mM MgCl₂ pH 7.5) using 10–20 μ g of protein supernatants. Assays were initiated by addition of succinyl-Leu-Leu-Val-Tyr-7-amido-4-methylcoumarin (Suc-LLVY-AMC, 100 μ M final concentration). This substrate is cleaved by the chymotrypsin-like (β_5) activity of the proteasome releasing free AMC, which was then measured spectrofluorometrically using a Fluoroskan Ascent fluorometer (Thermo Fisher Scientific) at an excitation wavelength of 390 nm and an emission wavelength of 460 nm. Fluorescence was measured at 15 minute intervals for 2 hours. All assays were linear in this range. Each assay was conducted in the absence and presence of the specific proteasomal inhibitor bortezomib (5

μM). The effect of the compounds on the 20S β_5 proteasomal activity of purified rabbit 20S proteasomes was performed in 50 mM Tris, pH 7.5. Compounds were incubated with proteasome for 20 minutes at room temperature before assaying for proteolytic activity [43].

Immunoblot Analysis

HepG2 cells were plated as similarly described above. Cells were then washed with cold PBS and lysed using cell lysis buffer [50 mM HEPES (pH 7.4), 4 mM EDTA, 100 mM sodium fluoride, 10 mM sodium pyrophosphate, 1% Triton X-100] containing protease and phosphatase inhibitors [100 mM phenylmethyl sulfonylfluoride (PMSF), 100 mM sodium orthovanadate, 1 mg/mL Aprotinin]. The cell lysates were centrifuged at 20,000 g for 15 minutes, and protein concentration was determined using BCA Protein Assay Reagent (Thermo Fisher Scientific). Twenty micrograms of protein from each sample was separated using SDS-PAGE gels and transferred onto PVDF Immobilon-P transfer membrane (Millipore). Polyubiquitination blot was performed using a combination of three antibodies: anti-ubiquitin (Sigma), anti-polyubiquitinated conjugates FK1 (Enzo Life Sciences), anti-ubiquitin P4D1 (Santa Cruz Biotechnology). The following antibodies were purchased from Cell Signaling Technology Inc.: anti-LC3B, anti-mTOR, anti-phospho-mTOR (Ser2448), anti-phospho-S6 kinase 1 (Ser371), anti-phospho-S6 kinase 1 (Thr389), anti-phospho-Akt (Thr308), anti-phospho-Akt (Ser473), anti-total-Akt, anti-phospho-PRAS40 (Thr246), anti-phospho-4E-BP1 (Thr31/46), anti-total-4E-BP1, anti-phospho-eIF2a (Ser51), anti-phospho-FOXO1 (Ser256), anti-IRE1 α , anti-GADPH, anti- β -actin, anti-tubulin and horseradish peroxidase (HRP)-conjugated secondary antibody. The following antibodies were purchased from EMD Millipore: anti-phospho-AMPK (Thr172), anti-4-HNE. The anti-BiP/GRP78 antibody was from BD Biosciences. The Division of Signaling Transduction Therapy (Dundee, Scotland) provided the anti-IRS1 antibodies. β -actin, Tubulin or GAPDH were used as loading controls as indicated. Blots were then developed with ECL Plus Western Blotting Detection System (GE Healthcare) and imaged using a Chemi Genius Bioimaging Gel Doc System (Syngene). All experiments were performed as previously described [44].

Kinase Selectivity Profile

Kinase screening was performed by Nanosyn using Microfluidic Technology as described by the company. Briefly, 0.1 mM stock solutions of the test compounds in DMSO were prepared. The solutions were diluted to a final concentration of 10 μM and tested in duplicate. The final concentration of DMSO in all assays was kept at 1%. Staurosporine and SB-202190 were assayed in 8-pt concentration response format in single wells/concentration. In all assays, ATP concentration corresponding to the K_M of the respective enzymes was used. Phosphorylation of substrates was detected using Caliper microfluidics mobility shift assay technology.

Statistical Analysis

Data were analyzed using One-Way Analysis of Variance (ANOVA) followed by Student-Newman-Keuls post-hoc analysis for pairwise multiple comparison, using Sigma Plot software suite. A p value <0.05 was considered statistically significant.

Results

***t*-AUCMB and *t*-MTUCB do not exhibit broad spectrum kinase inhibitory activities**

Our previous structure-activity relationship identified that *t*-AUCMB and *t*-MTUCB do not inhibit the primary targets of sorafenib, C-Raf kinase and VEGFR2 kinase [2]. Thus, we further explored their kinase inhibitory activities against a large panel of protein kinases. As expected, the multikinase inhibitory activity of sorafenib was observed, as this compound

significantly inhibiting 32% (23 of 72) of the kinases tested (10 μ M concentration). This includes many kinases not previously shown to be inhibited by sorafenib including Aurora-b kinase, DDR2, CSF1R, LynA, MAP4K5, MKNK2, RIPK2. Remarkably, neither of our analogues significantly inhibited any of the kinases tested in this panel (Figure 1). Our previous SAR study with a library of sorafenib-like compounds demonstrated that changes of the substituents on either side of the urea functional group in sorafenib, cause dramatic loss of inhibitory activity towards Raf kinase and VEGFR-2 [2]. However, the complete lack of kinase inhibitory activity against this panel of kinases was unexpected. Despite their structural similarities to sorafenib, these data demonstrated that *t*-AUCMB and *t*-MTUCB are highly selective compounds compared to sorafenib, and do not exhibit similar multi-kinase inhibitory activity.

***t*-AUCMB and *t*-MTUCB exhibit cytotoxicity across various cancer cell types**

Previously, *t*-AUCMB and *t*-MTUCB showed similar cytotoxicity to sorafenib on hepatoma cells [2]. We further tested if these analogues showed conserved cytotoxicity across other cancer cell types. *t*-AUCMB displayed consistent cytotoxicity across liver, kidney, prostate and breast cancer cell lines (Table 1). In contrast, *t*-MTUCB displayed a significant loss in cytotoxicity in both prostate and breast cancer lines (Table 1). Based on these data, and the fact that sorafenib is approved for hepatocellular carcinoma, liver cells (hepatoma cells) were chosen for further mechanistic investigations of these analogues.

***t*-AUCMB and *t*-MTUCB differentially induce caspase-dependent apoptosis and plasma membrane depolarization**

To elucidate the mechanism of cell death by *t*-AUCMB and *t*-MTUCB, a series of cell-based assays were performed to correlate cell viability, plasma membrane depolarization, and caspase 3/7 induction. *t*-AUCMB and *t*-MTUCB displayed distinct cellular responses in both hepatoma cell lines, HepG2 (Figure 2A) and Huh-7 (Figure 2B) cell lines. The cytotoxicity from *t*-AUCMB and sorafenib correlated with extensive lactate dehydrogenase (LDH) release and caspase 3/7 induction, suggestive of a late stage apoptotic event. However, cytotoxicity from *t*-MTUCB treatment was not associated with either caspase induction or LDH release. These data indicated that *t*-AUCMB and *t*-MTUCB induce two distinct patterns of cell death.

***t*-AUCMB and *t*-MTUCB do not affect cell cycle progression**

To determine whether the cell viability effects of *t*-AUCMB and *t*-MTUCB were associated with anti-proliferative responses, we compared their effects to sorafenib on cell cycle progression. Cell cycle analysis was performed with flow cytometry using the incorporation of EdU (5-ethynyl-2'-deoxyuridine) as an indicator of newly synthesized DNA. As expected, sorafenib-treated HepG2 cells showed significant arrest in G0/G1 phase after 24 hours of exposure. However, there was no significant effect of either analogue on cell cycle distribution (Figure 3). *t*-AUCMB and *t*-MTUCB thus do not exhibit anti-proliferative effects in hepatoma cells, which we surmise is a result from differences in kinase inhibitory activity.

***t*-AUCMB and *t*-MTUCB elicit mitochondrial membrane depolarization and apoptosis-inducing factor release**

The observed differences in caspase induction between *t*-AUCMB and *t*-MTUCB led to the question of whether caspase-independent events were involved in hepatoma cell death. Investigating the time dependency of cell viability showed that both compounds induced extensive cell death after only 6 hours of exposure (Figure 4A). We first examined the consequence of abolishing caspase activity using the pan-caspase inhibitor, Z-VAD-FMK,

and found no significant rescuing of cell viability with either sorafenib analogue (Figure 4A). The localization of apoptosis-inducing factor (AIF) was then investigated as an indication of mitochondrial depolarization [11; 12]. Under untreated conditions it was observed that this pro-apoptotic protein is localized in the mitochondria, as seen by the Alexa Fluor® 488 labeled AIF protein overlaying with the MitoTracker® Red labeled mitochondria (Figure 4B). However, extensive mitochondrial membrane depolarization occurred along with AIF release after exposure to both compounds. This was evidence that the cytotoxicity of both sorafenib analogues might be linked to mitochondrial membrane disruption.

The observation that *t*-MTUCB did not cause LDH release into the media of exposed cells (Figure 2), suggested that treatment with *t*-MTUCB was initiating mitochondrial membrane rupture without affecting the plasma membrane of these cells. To determine if this was an artifact of incubation time, extended treatment with *t*-MTUCB (72 hours) was performed. Interestingly, although the MTT assay [13] indicated there was little mitochondrial respiration (30% cell viability) after 72 hours, there was no observable LDH release into the media of *t*-MTUCB-treated cells (Figure 4C). Hypothesizing that *t*-MTUCB may be directly affecting LDH activity or LDH expression levels, the LDH activity was measured after washing the *t*-MTUCB-treated cell, followed by lysis with media containing 1% Triton X-100. Under these conditions there was a significant release of LDH activity into the lysis media (Figure 4C). HepG2 cell lysates were then incubated for 24 hours with both compounds to measure direct inhibition on LDH, and no effect on LDH enzymatic activity was observed (Figure 4C). These data indicated that *t*-MTUCB was not affecting LDH activity levels, but instead this compound possesses the unique ability to affect mitochondrial membrane disruption (thus cellular respiration and viability) without initiating plasma membrane rupture.

***t*-AUCMB and *t*-MTUCB induce autophagy**

Mitochondrial dysfunction has been shown to elicit autophagic responses [14], thus we investigated the ability of these compounds to induce autophagy. Following 6 hours of exposure at 30 μ M of *t*-AUCMB and *t*-MTUCB, extensive autophagosome vacuole formation was observed in HepG2 cells (Figure 5A). Autophagosome formation coincided with cleavage of LC3I to LC3II, confirming an autophagic response (Figure 5B). To investigate the nature of this autophagy, we first examined the effect of *t*-AUCMB and *t*-MTUCB on the activity of the mammalian target of rapamycin (mTOR) signaling pathway [15]. Unlike the classical mTOR-dependent autophagy inducer, rapamycin, we were unable to detect a decrease of phosphorylated form of mTOR, or its downstream targets, S6K1 and 4EBP1 (Figure 5C) for *t*-AUCMB. At the highest concentration of *t*-MTUCB (30 μ M), there appeared to be a reduction in the phosphorylation in mTOR and p-S6K1(371). This could be an indication that *t*-AUCMB and *t*-MTUCB differentially inhibit mTOR activity at high concentrations, however; *t*-MTUCB did not inhibit the phosphorylation of the mTOR substrate 4EBP1, suggesting this is unlikely.

It was clear however, that both *t*-AUCMB and *t*-MTUCB significantly amplified the levels of IRS1 protein, corresponding with an increase in phosphorylated protein kinase B (Akt) and its respective substrates, forkhead box protein (FOXO) [16] and the proline-rich Akt substrate 40 (PRAS40) [17]. To determine if mitochondrial dysfunction affected ATP output, we examined the phosphorylation of the metabolic regulator AMP-activated protein kinase (AMPK) [18], and found no observable increase in the phosphorylation of AMPK. This was an unexpected result as AMPK is an ATP-sensor, sensitive to changes in cellular AMP:ATP and ADP:ATP ratios. We suspect that ATP is likely predominately generated from glycolysis in these liver cells and thus changes in mitochondrial ATP production may

not be sufficient to cause an AMPK response. Nonetheless, these data indicated that signaling downstream of the mTORC1 pathway was unaffected by treatment with *t*-AUCMB and thus the observed autophagy induced by *t*-AUCMB appears to be an mTORC1-independent event. With regards to *t*-MTUCB, it is unclear if at high concentration this compound truly inhibits the phosphorylation of mTOR(2448) resulting in differential effects on phosphorylation of the two mTORC1 substrates, S6K1 and 4EBP1. Further binding studies are required, but the fact that there was no indication of kinase inhibitory activity in the kinase screening panel, and both analogues exhibit similar upstream activation, suggests this is an unlikely event.

To determine whether the autophagy induced by *t*-AUCMB and *t*-MTUCB was involved in cell death, HepG2 cells were co-treated with a chemical inhibitor of autophagy, chloroquine [19]. Co-treatment with chloroquine neither potentiated nor attenuated the cytotoxic responses of these compounds at the time point of the observed autophagy induction (6 hours) (Figure 5D). Therefore, cell death does not appear to be proceeding through an autophagic mechanism.

***t*-AUCMB and *t*-MTUCB induce endoplasmic reticulum-independent oxidative stress**

To further elucidate the underlying cause of the autophagy, we examined the changes in glutathione levels upon treatment of HepG2 cells with *t*-AUCMB and *t*-MTUCB. After 6 hours of incubation there was a significant depletion of the reduced form of glutathione (GSH) and a nearly two-fold increase of the oxidized form (GSSG) (Figure 6A). Based on the relationship between cellular redox potential and endoplasmic reticulum stress (ER) [20], two markers for ER stress, binding immunoglobulin protein (BiP) [21] and inositol-requiring enzyme-1 α (IRE1 α) [22; 23], were analyzed by western blot. However, there was no observable change in the expression levels of these proteins following treatment with either *t*-AUCMB or *t*-MTUCB (Figure 6B). We then examined changes in the phosphorylation state of the eukaryotic initiation factor 2 α (eIF2 α) as an indication of ER-stress-induced PERK [PKR (double-stranded-RNA-dependent protein kinase)-like ER kinase] activity [24]. Sorafenib significantly increased the p-eIF2 α levels in HepG2 cells as seen previously in human leukemia cells [20], whereas this effect was not observed in cells treated with either *t*-AUCMB or *t*-MTUCB (Figure 6B). Finally, we performed western blot analysis of 4-hydroxynonenal (4-HNE) as an indicator of ROS-induced lipid peroxidation [25], and also observed no significant changes (Figure 6B). Taken together, these data indicated that the effects of *t*-AUCMB and *t*-MTUCB on glutathione levels are independent of ER-mediated and lipid-mediated oxidative stress.

To determine whether glutathione depletion was linked to the cytotoxicity, both *t*-AUCMB and *t*-MTUCB were co-incubated with the two ROS scavengers, α -tocopherol (α TP) and *N*-acetyl-cysteine (NAC). Consistent with our 4-HNE data, co-treatment with the lipid peroxide scavenger, α TP, had no effect on the cell viability effects of our compounds (Figure 6C). However, co-treatment with NAC significantly attenuated the cytotoxicity of both compounds, and completely recovered the cell viability effects of *t*-AUCMB. This provided strong evidence that the depletion of GSH levels is directly linked to the cytotoxicity of these compounds.

Induction of autophagy by *t*-AUCMB and *t*-MTUCB is not through inhibition of proteasome activity

Proteasome activity is known to be sensitive to oxidative stress [26], prompting the further investigation of the effects of these compounds on the ubiquitin-proteasome system. We observed a significant decrease in the cellular beta 5 (chymotrypsin-like) proteasome activity after 6 hours of incubation with *t*-AUCMB in HepG2 cells, and both compounds

further suppressed proteasome activity after 24 hours (Figure 7A). However, incubation of up to 25 μ M of either compound failed to directly inhibit the activity of purified beta 5 proteasome (data not shown).

Since an increase in ubiquitinated proteins through proteasome inhibition can lead to autophagy and cell death [27], we then asked whether our compounds affected the total ubiquitinated protein levels after 6 hours of treatment (Figure 7B). Although the data was only found to be significant for *t*-AUCMB, all three compounds tended to decrease, rather than an expected increase, in polyubiquitination. This indicated that even though our compounds indirectly suppress proteasome activity, it does not lead to an increase in ubiquitinated protein levels in the time frame of cell death and the observed autophagy. Thus, the indirect inhibition of proteasome activity was responsible for induction of autophagy.

Finally, we asked whether modulation of proteasome activity with proteasome inhibitor (MG132 [28] or bortezomib [29]) or proteasome activator (oleuropein [30]) in combination with our compounds affected cell viability. We found that modulation of proteasome activity with chemical mediators neither potentiated nor attenuated the cell viability responses of *t*-AUCMB and *t*-MTUCB (Figure 7C). These data strongly indicate that the effects on the ubiquitin-proteasome system are not linked to the cytotoxicity of these compounds, rather likely a result from changes in the reduction potential in the cell from the glutathione depletion.

Discussion

From a library of previously published sorafenib analogues we found two cytotoxic compounds, *t*-AUCMB and *t*-MTUCB, which exhibited similar potency on hepatoma cells to sorafenib, despite their differences in inhibition profiles against known sorafenib targets [2]. Sorafenib exhibits many different cellular and programmed cell death responses including caspase-dependent [31] and caspase-independent apoptosis [32], mitochondrial dysfunction [33], anti-proliferation [34], mTOR-dependent autophagy [35], ER-mediated stress [20] and oxidative stress [36]. In this report, we examined each of these cellular responses for our two novel sorafenib analogues and found they differentially affect apoptosis.

Although all compounds have similar cytotoxicity, *t*-AUCMB and *t*-MTUCB exhibit unique hepatoma cellular responses not only when compared to sorafenib, but also between each other. *t*-AUCMB is similar to sorafenib in the ability to induce caspase activation and plasma membrane depolarization in hepatoma cells, whereas the effect on cell viability from the treatment with *t*-MTUCB is independent of both these traditionally apoptotic events. These were puzzling results since both apoptosis and necrosis typically lead to plasma membrane depolarization and cellular content leakage *in vitro* [37; 38]. Incubation of cell lysates with *t*-MTUCB does not affect LDH enzyme activity, and the lysis of cells pre-treated with *t*-MTUCB releases significant amount of LDH into the media. Based on these two observations it was clear that *t*-MTUCB does not directly inhibit LDH, nor suppresses LDH transcriptional regulation. Thus, these observations were not an artifact of the LDH assay. In addition, there was no observable effect on cell cycle progression with either analogue, suggesting that senescence is not accountable. Thus, *t*-MTUCB appears to display the unique ability to affect cellular respiration and cell viability, independent of plasma membrane rupture.

The link between mitochondrial function and autophagy has been well established [39; 40]. Here we observed that both analogues significantly induced autophagy in HepG2 cells and coinciding with mitochondrial depolarization. However, unlike sorafenib inhibition of the

mTOR signaling pathway was not observed [35]. In addition to our western blot data, kinase screening demonstrated that many of kinases known to be involved in mTOR signaling are not inhibited by these analogues, providing convincing evidence these compounds are inducing mTOR-independent autophagy.

Based on these findings, we first asked whether this autophagy affects the cytotoxicity of these compounds as previously observed for sorafenib [35]. If the induced autophagy is contributing to, or protecting the cells from, programmed cell death, then the inhibition of autophagy should either attenuate or potentiate the effects on cell death, respectively. Since the co-treatment with chloroquine did not affect cell viability, we hypothesize that the observed autophagic response induced by our compounds is either not playing a major role in the cell death, or that these compounds induce cellular functional alterations in which autophagy (or the inhibition of autophagy) cannot rescue. Examining oxidative stress as possible causes of the mTOR-independent autophagy, led to the observation that all three compounds significantly shifted the glutathione species towards the oxidized form. The addition of exogenous NAC rescued cell viability with both analogues, demonstrating that the glutathione depletion may be directly linked the cell viability effects and to mitochondrial dysfunction. However, the effect on glutathione depletion was not associated an increase in the ER-stress related markers, BiP and IRE1 α , suggesting that *t*-AUCMB and *t*-MTUCB induce ER-independent oxidative stress. To further verify ER-independent stress related events, we then examined the effects on p-eIF2 α levels as a marker of PERK-dependent inhibition of protein synthesis [24]. Consistent with previous observations in leukemia cells [20], sorafenib treatment significantly increased p-eIF2 levels in HepG2 cells but this was not observed for either analogue.

Finally, since the ubiquitin-proteasome system is known to be highly sensitive to oxidative stress [26] which can lead to the induction of autophagy [41], we examined the effects of *t*-AUCMB and *t*-MTUCB on beta 5 proteasome activity and polyubiquitination. Treatment with our analogues indirectly suppressed cellular proteasome activity, but neither compound affected total ubiquitinated protein at the time of autophagy induction. Therefore, cellular stress from an excess of ubiquitinated protein was not responsible for the observed autophagy, but rather proteasome function is most likely being modulated by the induced oxidative stress from the treatment of these compounds.

In summary, *t*-AUCMB and *t*-MTUCB are two novel sorafenib-based analogues that induce mTOR-independent autophagy, but result in divergent apoptotic events (caspase activation and LDH release). The downstream responses (i.e., autophagy, cellular redox changes, and indirect inhibition of the proteasome) are identical for these compounds, which may indicate that the structural differences for *t*-AUCMB induces added conventional apoptotic responses compared to *t*-MTUCB. Based on the structural similarities between these two compounds, it is likely that the adamantyl group in *t*-AUCMB is the chemical moiety responsible for the differences in their apoptotic responses. In addition, *t*-AUCMB showed superior cytotoxicity on prostate and breast cancer cell lines, suggesting the lipophilic adamantyl group may be targeting certain pathways critical for cellular survival in these cancer types. However, the mechanism by which *t*-MTUCB effects mitochondrial membrane integrity (thus cellular respiration) without plasma membrane disruption is further being investigated. *t*-AUCMB and *t*-MTUCB are unique sorafenib-based structural analogues which exhibit strong cytotoxicity in a variety of cancer cell lines, and potentially valuable tools for probing the cross-talk between mitochondrial-induced apoptosis and autophagy.

Acknowledgments

We thank Dr. Michael Praddy of the MCB Imaging Facility for help with collecting and analyzing our immunohistochemical data on the Olympus FV100 laser point scanning microscope. Special thanks to the Dawson laboratory for the use of their Leica DMI6000 B inverted fluorescence microscope to collect live-cell autophagosome imaging, and to Carol Oxford and the UCD Flow Cytometry Shared Resource facility for help with collecting and analyzing cell cycle data. We also thank the Buckpitt lab for help with glutathione quantification.

Grant information

This work was supported in part by NIEHS grant ES02710, NIEHS Superfund grant P42 ES04699, and NIH grant HL059699 (all to B.D.H.). This work was also supported by NIH grants 5U01CA86402 (Early Detection Research Network), 1R01CA135401-01A1, and 1R01DK082690-01A1 (all to R.H.W.), and the Medical Service of the US Department of Veterans' Affairs (R.H.W.). A.V.G was supported in part by NHLBI grant HL096819. A.T.W. was supported by Award Number T32CA108459 from the National Institutes of Health. B.D.H. is a George and Judy Marcus senior fellow of the American Asthma Foundation.

Abbreviations List

HCC	hepatocellular carcinoma
sEH	soluble epoxide hydrolase
mTOR	mammalian target of rapamycin
<i>t</i>-MTUCB	<i>trans</i> - <i>N</i> -methyl-4-[4-[3-(4-trifluoromethoxy-phenyl)-ureido]-cyclohexyloxy]-benzamide
<i>t</i>-AUCMB	<i>trans</i> -4-[4-(3-adamantan-1-yl-ureido)-cyclohexyloxy]- <i>N</i> -methyl-benzamide

References

- Liu JY, Park SH, Morisseau C, Hwang SH, Hammock BD, Weiss RH. Sorafenib has soluble epoxide hydrolase inhibitory activity, which contributes to its effect profile in vivo. *Mol Cancer Ther.* 2009; 8:2193–2203. [PubMed: 19671760]
- Hwang SH, Weckslers AT, Zhang G, Morisseau C, Nguyen LV, Fu SH, Hammock BD. Synthesis and Biological Evaluation of Sorafenib- and Regorafenib-like sEH Inhibitors. *Bioorg Med Chem Lett.* 2013; 23:3732–3737. [PubMed: 23726028]
- Chen KF, Chen HL, Tai WT, Feng WC, Hsu CH, Chen PJ, Cheng AL. Activation of phosphatidylinositol 3-kinase/Akt signaling pathway mediates acquired resistance to sorafenib in hepatocellular carcinoma cells. *J Pharmacol Exp Ther.* 2011; 337:155–161. [PubMed: 21205925]
- Laplanche M, Sabatini DM. mTOR signaling at a glance. *J Cell Sci.* 2009; 122:3589–3594. [PubMed: 19812304]
- Decuyper JP, Bultynck G, Parys JB. A dual role for Ca(2+) in autophagy regulation. *Cell Calcium.* 2011; 50:242–250. [PubMed: 21571367]
- Mihaylova MM, Shaw RJ. The AMPK signalling pathway coordinates cell growth, autophagy and metabolism. *Nat Cell Biol.* 2011; 13:1016–1023. [PubMed: 21892142]
- Frank M, Duvezin-Caubet S, Koob S, Occhipinti A, Jagasia R, Petcherski A, Ruonala MO, Priault M, Salin B, Reichert AS. Mitophagy is triggered by mild oxidative stress in a mitochondrial fission dependent manner. *Biochim Biophys Acta.* 2012; 1823:2297–2310. [PubMed: 22917578]
- Kiffin R, Bandyopadhyay U, Cuervo AM. Oxidative stress and autophagy. *Antioxid Redox Signal.* 2006; 8:152–162. [PubMed: 16487049]
- Wu WK, Sakamoto KM, Milani M, Aldana-Masangkay G, Fan D, Wu K, Lee CW, Cho CH, Yu J, Sung JJ. Macroautophagy modulates cellular response to proteasome inhibitors in cancer therapy. *Drug Resist Updat.* 2010; 13:87–92. [PubMed: 20462785]
- Chen S, Rehman SK, Zhang W, Wen A, Yao L, Zhang J. Autophagy is a therapeutic target in anticancer drug resistance. *Biochim Biophys Acta.* 2010; 1806:220–229. [PubMed: 20637264]

11. Joza N, Susin SA, Daugas E, Stanford WL, Cho SK, Li CY, Sasaki T, Elia AJ, Cheng HY, Ravagnan L, Ferri KF, Zamzami N, Wakeham A, Hakem R, Yoshida H, Kong YY, Mak TW, Zuniga-Pflucker JC, Kroemer G, Penninger JM. Essential role of the mitochondrial apoptosis-inducing factor in programmed cell death. *Nature*. 2001; 410:549–554. [PubMed: 11279485]
12. Norberg E, Orrenius S, Zhivotovsky B. Mitochondrial regulation of cell death: processing of apoptosis-inducing factor (AIF). *Biochem Biophys Res Commun*. 2010; 396:95–100. [PubMed: 20494118]
13. Mosmann T. Rapid colorimetric assay for cellular growth and survival: application to proliferation and cytotoxicity assays. *J Immunol Methods*. 1983; 65:55–63. [PubMed: 6606682]
14. Lemasters JJ, Nieminen AL, Qian T, Trost LC, Elmore SP, Nishimura Y, Crowe RA, Cascio WE, Bradham CA, Brenner DA, Herman B. The mitochondrial permeability transition in cell death: a common mechanism in necrosis, apoptosis and autophagy. *Biochim Biophys Acta*. 1998; 1366:177–196. [PubMed: 9714796]
15. Diaz-Troya S, Perez-Perez ME, Florencio FJ, Crespo JL. The role of TOR in autophagy regulation from yeast to plants and mammals. *Autophagy*. 2008; 4:851–865. [PubMed: 18670193]
16. Smolewski P. Recent developments in targeting the mammalian target of rapamycin (mTOR) kinase pathway. *Anticancer Drugs*. 2006; 17:487–494. [PubMed: 16702804]
17. Vander Haar E, Lee SI, Bandhakavi S, Griffin TJ, Kim DH. Insulin signalling to mTOR mediated by the Akt/PKB substrate PRAS40. *Nat Cell Biol*. 2007; 9:316–323. [PubMed: 17277771]
18. Gwinn DM, Shackelford DB, Egan DF, Mihaylova MM, Mery A, Vasquez DS, Turk BE, Shaw RJ. AMPK phosphorylation of raptor mediates a metabolic checkpoint. *Mol Cell*. 2008; 30:214–226. [PubMed: 18439900]
19. Solomon VR, Lee H. Chloroquine and its analogs: a new promise of an old drug for effective and safe cancer therapies. *Eur J Pharmacol*. 2009; 625:220–233. [PubMed: 19836374]
20. Rahmani M, Davis EM, Crabtree TR, Habibi JR, Nguyen TK, Dent P, Grant S. The kinase inhibitor sorafenib induces cell death through a process involving induction of endoplasmic reticulum stress. *Mol Cell Biol*. 2007; 27:5499–5513. [PubMed: 17548474]
21. Lee J, Giordano S, Zhang J. Autophagy, mitochondria and oxidative stress: cross-talk and redox signalling. *Biochem J*. 2012; 441:523–540. [PubMed: 22187934]
22. Kohno K, Normington K, Sambrook J, Gething MJ, Mori K. The promoter region of the yeast KAR2 (BiP) gene contains a regulatory domain that responds to the presence of unfolded proteins in the endoplasmic reticulum. *Mol Cell Biol*. 1993; 13:877–890. [PubMed: 8423809]
23. Lee K, Tirasophon W, Shen X, Michalak M, Prywes R, Okada T, Yoshida H, Mori K, Kaufman RJ. IRE1-mediated unconventional mRNA splicing and S2P-mediated ATF6 cleavage merge to regulate XBP1 in signaling the unfolded protein response. *Genes Dev*. 2002; 16:452–466. [PubMed: 11850408]
24. Harding HP, Zhang Y, Ron D. Protein translation and folding are coupled by an endoplasmic-reticulum-resident kinase. *Nature*. 1999; 397:271–274. [PubMed: 9930704]
25. Awasthi YC, Sharma R, Sharma A, Yadav S, Singhal SS, Chaudhary P, Awasthi S. Self-regulatory role of 4-hydroxynonenal in signaling for stress-induced programmed cell death. *Free Radic Biol Med*. 2008; 45:111–118. [PubMed: 18456001]
26. Aiken CT, Kaake RM, Wang X, Huang L. Oxidative stress-mediated regulation of proteasome complexes. *Mol Cell Proteomics*. 2011; 10:R110.006924.
27. Ge PF, Zhang JZ, Wang XF, Meng FK, Li WC, Luan YX, Ling F, Luo YN. Inhibition of autophagy induced by proteasome inhibition increases cell death in human SHG-44 glioma cells. *Acta Pharmacol Sin*. 2009; 30:1046–1052. [PubMed: 19575007]
28. Tsubuki S, Kawasaki H, Saito Y, Miyashita N, Inomata M, Kawashima S. Purification and characterization of a Z-Leu-Leu-Leu-MCA degrading protease expected to regulate neurite formation: a novel catalytic activity in proteasome. *Biochem Biophys Res Commun*. 1993; 196:1195–1201. [PubMed: 8250877]
29. Teicher BA, Ara G, Herbst R, Palombella VJ, Adams J. The proteasome inhibitor PS-341 in cancer therapy. *Clin Cancer Res*. 1999; 5:2638–2645. [PubMed: 10499643]

30. Katsiki M, Chondrogianni N, Chinou I, Rivett AJ, Gonos ES. The olive constituent oleuropein exhibits proteasome stimulatory properties in vitro and confers life span extension of human embryonic fibroblasts. *Rejuvenation Res.* 2007; 10:157–172. [PubMed: 17518699]
31. Huang R, Chen XQ, Huang Y, Chen N, Zeng H. The multikinase inhibitor sorafenib induces caspase-dependent apoptosis in PC-3 prostate cancer cells. *Asian J Androl.* 2010; 12:527–534. [PubMed: 20473320]
32. Panka DJ, Wang W, Atkins MB, Mier JW. The Raf inhibitor BAY 43-9006 (Sorafenib) induces caspase-independent apoptosis in melanoma cells. *Cancer Res.* 2006; 66:1611–1619. [PubMed: 16452220]
33. Chiou JF, Tai CJ, Wang YH, Liu TZ, Jen YM, Shiao CY. Sorafenib induces preferential apoptotic killing of a drug- and radio-resistant Hep G2 cells through a mitochondria-dependent oxidative stress mechanism. *Cancer Biol Ther.* 2009; 8:1904–1913. [PubMed: 19770576]
34. Wilhelm S, Carter C, Lynch M, Lowinger T, Dumas J, Smith RA, Schwartz B, Simantov R, Kelley S. Discovery and development of sorafenib: a multikinase inhibitor for treating cancer. *Nat Rev Drug Discov.* 2006; 5:835–844. [PubMed: 17016424]
35. Shimizu S, Takehara T, Hikita H, Kodama T, Tsunematsu H, Miyagi T, Hosui A, Ishida H, Tatsumi T, Kanto T, Hiramatsu N, Fujita N, Yoshimori T, Hayashi N. Inhibition of autophagy potentiates the antitumor effect of the multikinase inhibitor sorafenib in hepatocellular carcinoma. *Int J Cancer.* 2011; 131:548–557. [PubMed: 21858812]
36. Coriat R, Nicco C, Chereau C, Mir O, Alexandre J, Ropert S, Weill B, Chaussade S, Goldwasser F, Batteux F. Sorafenib-induced hepatocellular carcinoma cell death depends on reactive oxygen species production in vitro and in vivo. *Mol Cancer Ther.* 2012; 11:2284–2293. [PubMed: 22902857]
37. Decker T, Lohmann-Matthes ML. A quick and simple method for the quantitation of lactate dehydrogenase release in measurements of cellular cytotoxicity and tumor necrosis factor (TNF) activity. *J Immunol Methods.* 1988; 115:61–69. [PubMed: 3192948]
38. Bouchier-Hayes L, Munoz-Pinedo C, Connell S, Green DR. Measuring apoptosis at the single cell level. *Methods.* 2008; 44:222–228. [PubMed: 18314052]
39. Rambold AS, Lippincott-Schwartz J. Mechanisms of mitochondria and autophagy crosstalk. *Cell Cycle.* 2011; 10:4032–4038. [PubMed: 22101267]
40. Wang K, Klionsky DJ. Mitochondria removal by autophagy. *Autophagy.* 2011; 7:297–300. [PubMed: 21252623]
41. Wong E, Cuervo AM. Integration of clearance mechanisms: the proteasome and autophagy. *Cold Spring Harb Perspect Biol.* 2010; 12:a006734. [PubMed: 21068151]
42. Lakritz J, Plopper CG, Buckpitt AR. Validated high-performance liquid chromatography-electrochemical method for determination of glutathione and glutathione disulfide in small tissue samples. *Anal Biochem.* 1997; 247:63–68. [PubMed: 9126372]
43. Gomes AV, Waddell DS, Siu R, Stein M, Dewey S, Furlow JD, Bodine SC. Upregulation of proteasome activity in muscle RING finger 1-null mice following denervation. *FASEB J.* 2012; 26:2986–2999. [PubMed: 22508689]
44. Inoue H, Hwang SH, Weckler AT, Hammock BD, Weiss RH. Sorafenib attenuates p21 in kidney cancer cells and augments cell death in combination with DNA-damaging chemotherapy. *Cancer Biol Ther.* 2011; 12:827–836. [PubMed: 21878748]

Kinase	<i>t</i> -AUCMB	<i>t</i> -MTUCB	Sorafenib	Kinase	<i>t</i> -AUCMB	<i>t</i> -MTUCB	Sorafenib
Abl	-4	1	94	LynA	1	2	97
AKT3	2	3	1	MAP4K5	0	9	93
ALK	2	2	8	MAPK1 (ERK2)	1	2	0
AURORA-A	-1	2	73	MEK1	2	3	15
AURORA-B	1	4	96	MET	0	0	0
Axl	2	-2	68	MNK2 (MKNK2)	-10	-5	96
BMX	1	2	22	NEK2	-1	2	4
BTK	3	3	38	p38alpha (MAPK14)	-1	-3	99
CAMK1D	-2	0	37	p38delta (MAPK13)	-1	-1	37
CDK2/cyclinA	-3	-4	15	p70S6K1	0	1	63
CHEK1	2	4	2	PAK1	-14	-13	-17
CK1a	1	1	2	PAK4	10	2	-4
CRAF	1	1	100	PDGFRa	2	1	100
CSK	2	4	71	PDGFRb	-1	2	100
DDR2	-4	-3	99	PDK1	0	0	0
DYRK1a	6	10	14	PI3Ka	18	26	93
EGFR	0	3	8	PIM-2	1	12	3
EphA3	-8	-9	81	PKA	0	0	2
EphB3	-1	-3	19	PKCalpha	4	-1	0
ErbB4 (HER4)	-2	3	3	PLK1	-1	3	5
FGFR3	1	0	86	PRKG2	1	0	17
Flt-1 (VEGFR1)	0	0	100	FAK2 (PTK2)	1	1	15
Flt-3	-6	4	98	RET	3	4	101
FMS (CSF1R)	1	4	104	RIPK2	0	0	92
Fyn	-3	2	81	ROCK1	0	1	27
GSK3alpha	15	9	0	ROS	-1	-1	30
GSK3beta	0	1	41	SGK1	3	0	5
IGF1R	6	2	2	SRC	-1	1	65
IKKb	5	1	4	SYK	-13	-11	-15
InsR	0	-4	-2	TBK1	0	0	1
IRAK4	1	2	3	TNK2	-5	-3	-1
JAK2	8	-2	31	TRKA (NTRK1)	-1	2	98
JNK2	4	5	65	TTK	-6	-5	67
KDR (VEGFR2)	-4	-1	98	TYRO3	1	2	70
c-Kit	3	5	99	ZAP70	-12	-11	-8
LCK	4	3	91	SPHK1	-2	-2	0

Figure 1. Selectivity profiles of *t*-AUCMB and *t*-MTUCB compared to sorafenib. Assays were performed at 10 μ M test concentrations. Red > 80% inhibition (strong inhibition), Yellow 40–80% inhibition (moderate inhibition), Green >40% inhibition (no significant inhibition). Data was generated by Nanosyn (Santa Clara, CA).

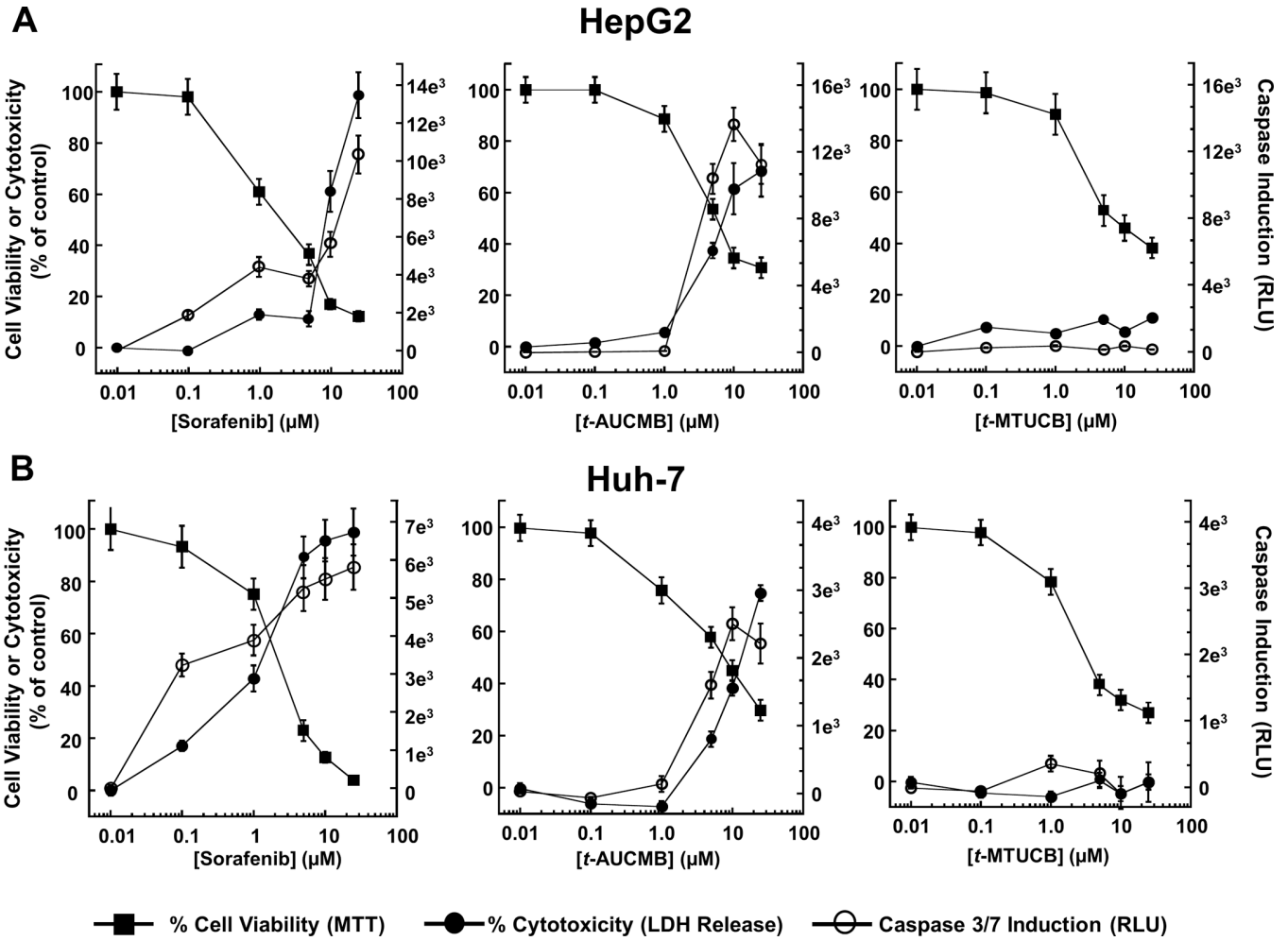


Figure 2. *t*-AUCMB and *t*-MTUCB differentially induce apoptosis and plasma membrane rupture in hepatoma cells
 The effects of *t*-AUCMB and *t*-MTUCB on cytotoxicity (MTT), plasma membrane depolarization (LDH activity), and caspase-dependent apoptosis (caspase 3/7 induction) on HepG2 (A) and Huh-7 (B) hepatoma cells. Data were determined after a 72 hour treatment period for each compound.

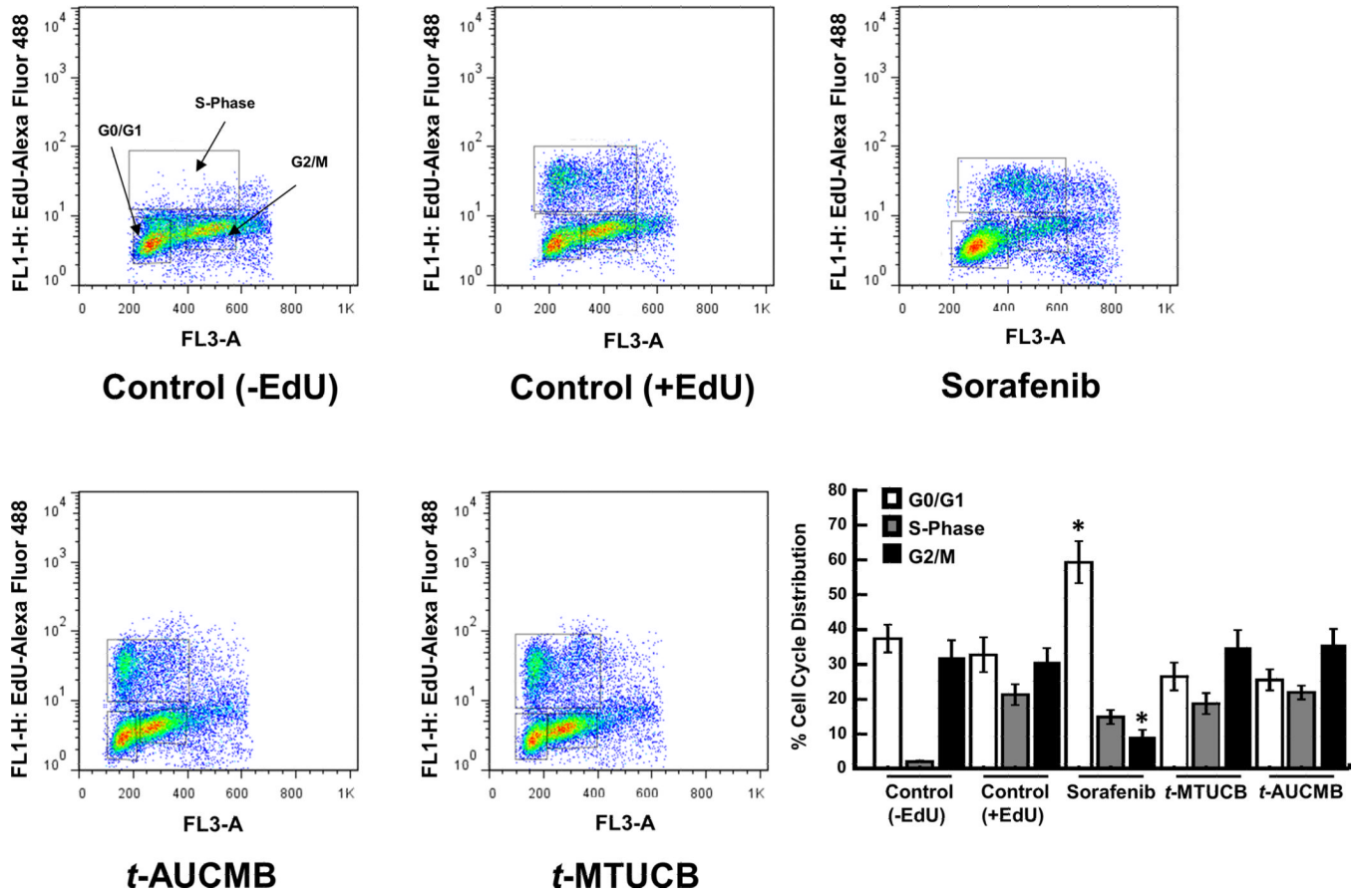


Figure 3. *t*-AUCMB and *t*-MTUCB do not exhibit anti-proliferative activities

Cell cycle analysis comparison to sorafenib in HepG2 cells after exposure for 24 hours at 30 μ M (n = 3). No significant effects on cell cycle progression were observed with *t*-AUCMB or *t*-MTUCB treatment. * P value <0.05 as compared to DMSO control (+EdU).

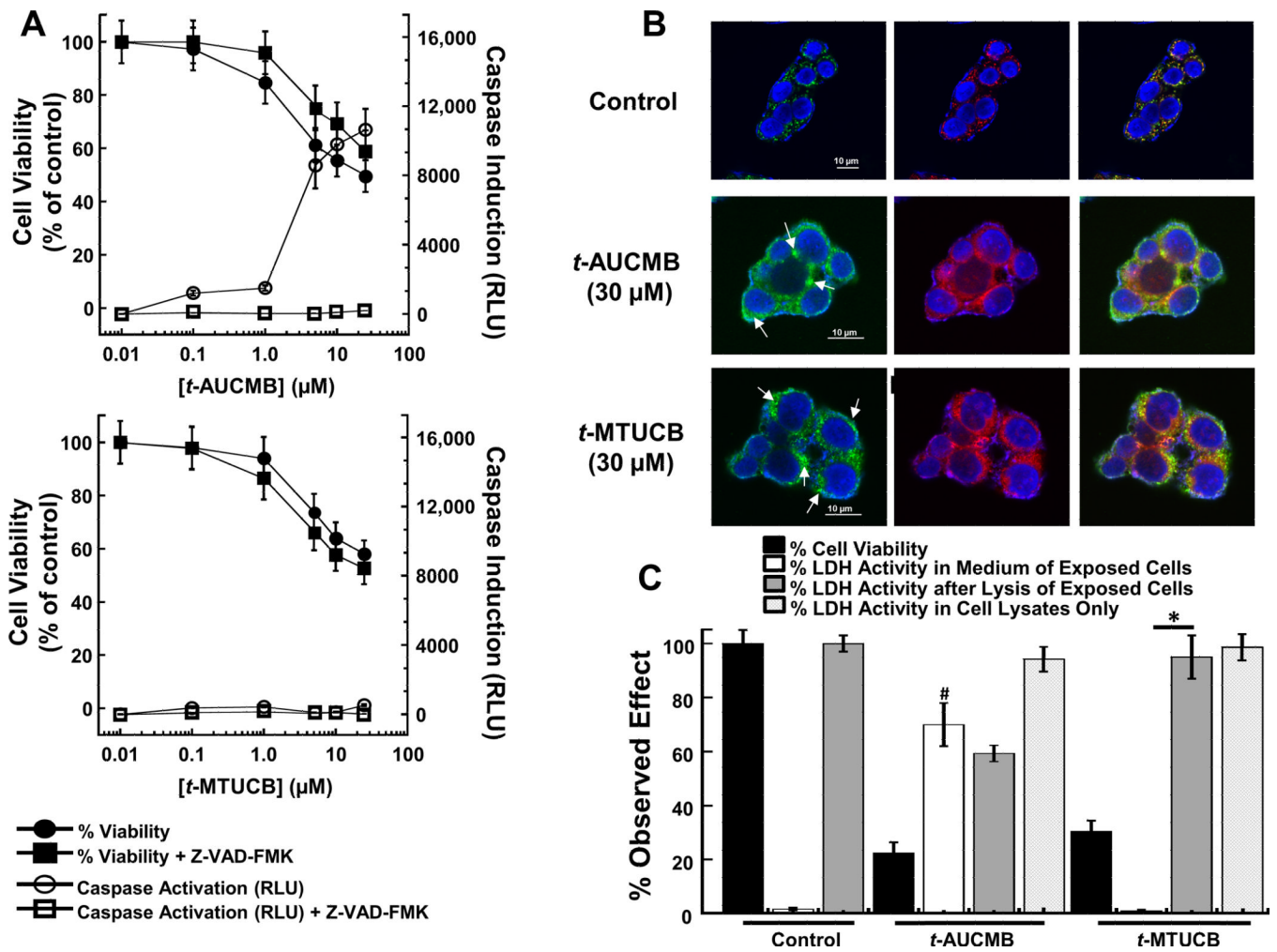


Figure 4. *t*-AUCMB and *t*-MTUCB induce mitochondrial depolarization

(A) The effects on HepG2 cell viability by *t*-AUCMB or *t*-MTUCB co-treated with Z-VAD-FMK (20 μ M) after 6 hours treatment. (B) Mitochondrial depolarization and AIF nuclear release after HepG2 exposure for 6 hours at 30 μ M. Arrows indicating AIF accumulation. (C) Comparison of lactate dehydrogenase release and activity in the media of treated cells (72 hours), cell lysis of treated cells (72 hours), and cell lysates alone (24 hours incubation in cell lysates). No direct LDH inhibition was observed by either compound. * P value < 0.05 as compared to DMSO control and # P value < 0.05 as compared to no cell lysis.

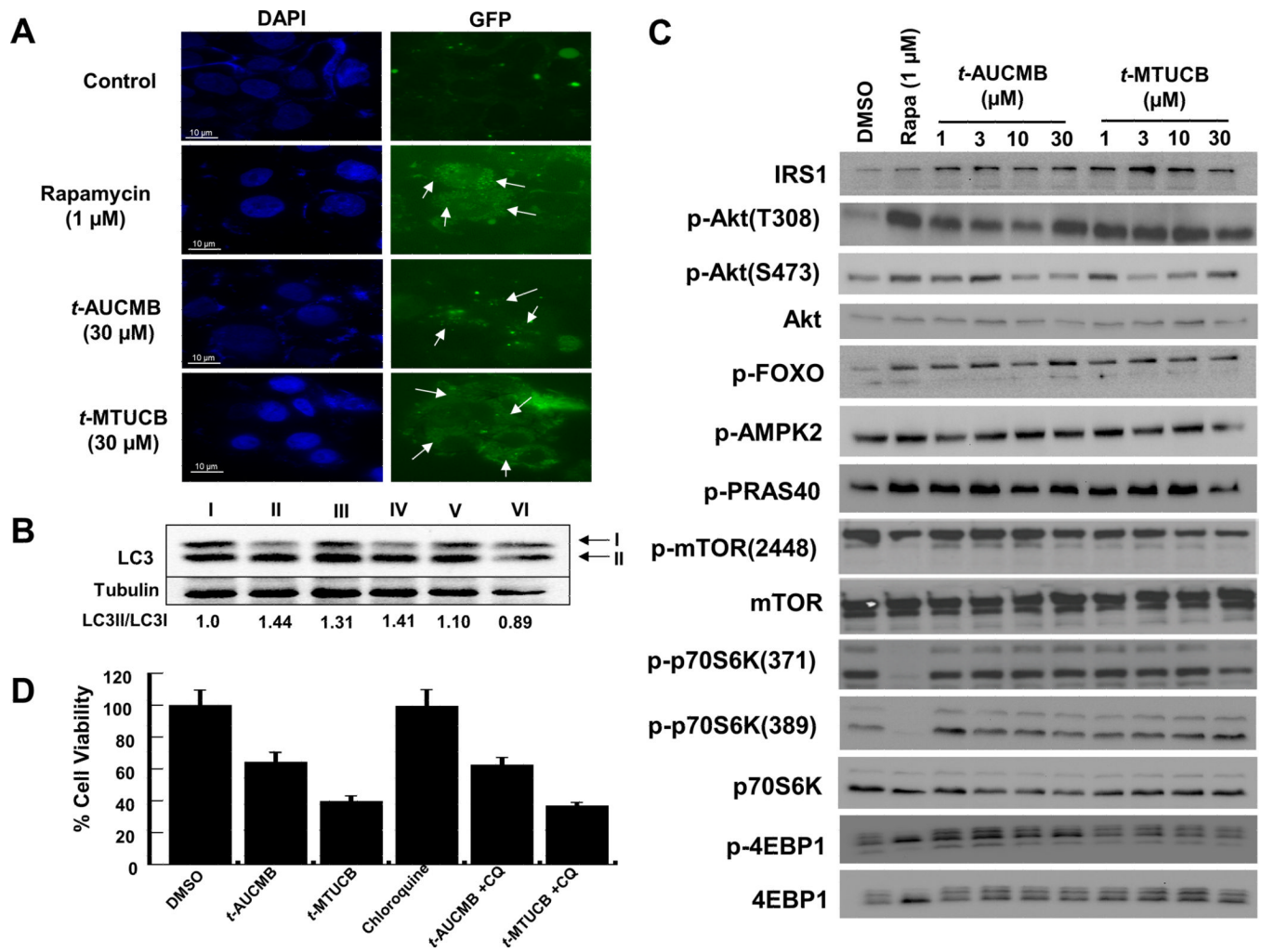


Figure 5. *t*-AUCMB and *t*-MTUCB induce mTOR-independent autophagy

(A) Fluorescence visualization of autophagosomal vacuole formation after 6 hours treatment. (B) Western blot data of LC3 cleavage and densitometry ratios of LC3II/LC3I. Samples: I = DMSO, II = *t*-AUCMB (30 μ M), III = *t*-MTUCB (30 μ M), IV = rapamycin (1 μ M) (positive control), V = tamoxifen (1 μ M) (positive control), VI = chloroquine (25 μ M) (negative control). Tubulin was used as loading control. (C) Western blot of the effects of *t*-AUCMB and *t*-MTUCB on the mTOR-signaling pathway. All data was collected after 6 hours exposure of HepG2 cells to the indicated concentrations of *t*-AUCMB and *t*-MTUCB. (D) Cell viability responses upon co-treatment with chloroquine (25 μ M) after 6 hours treatment. No significant differences were observed.

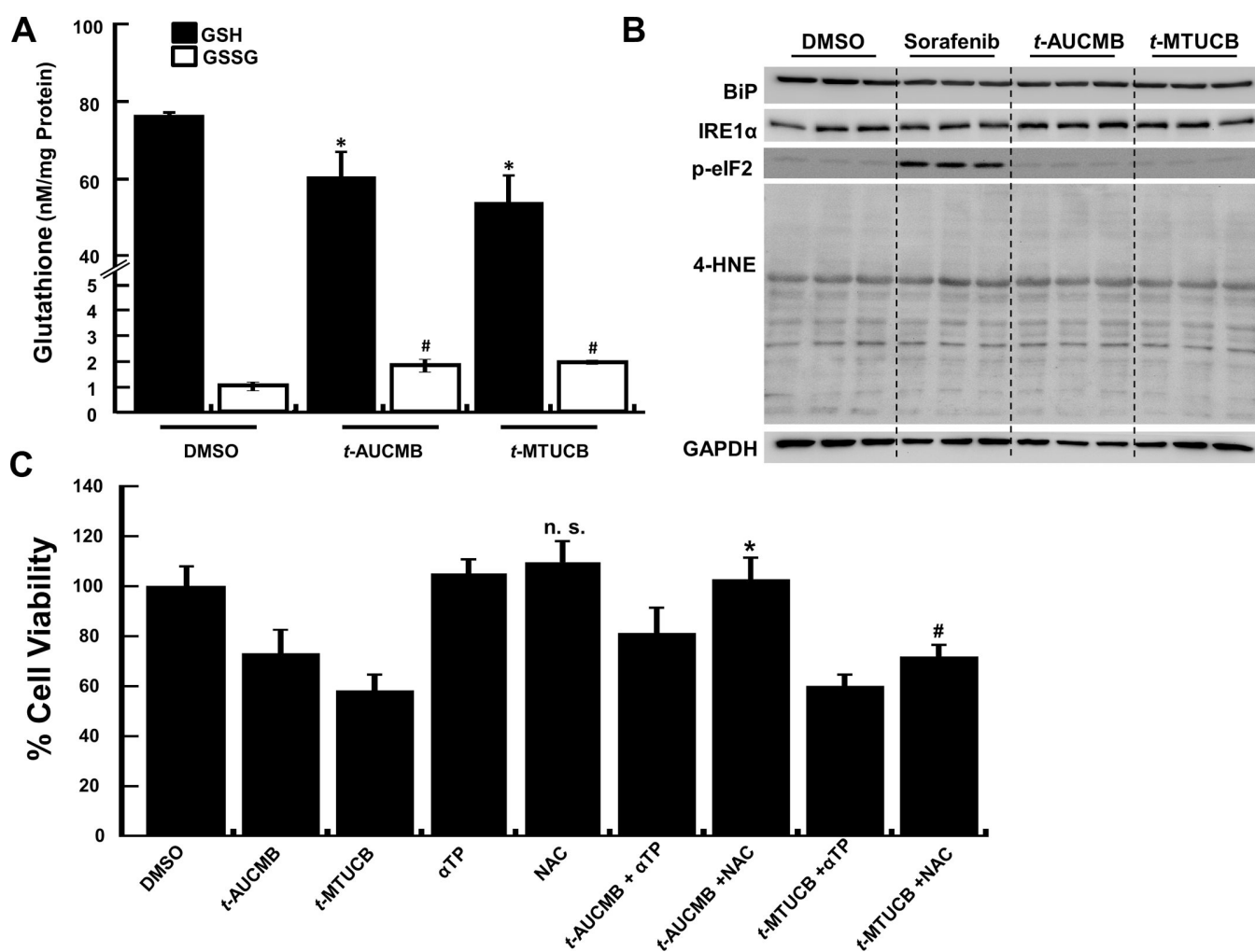


Figure 6. *t*-AUCMB and *t*-MTUCB induce ER-independent oxidative stress

(A) Effects on glutathione concentrations. **P* value <0.05 as compared to DMSO (GSH). #*P* value <0.05 as compared to DMSO control (GSSG). (B) Western blot analysis of ER-stress and lipid oxidation markers. (C) HepG2 Cell viability responses upon co-treatment with ROS scavengers, α-tocopherol (10 μM) and N-acetyl-cysteine (5 mM). GAPDH was used as loading control. **P* value <0.05 as compared *t*-AUCMB alone. #*P* value <0.05 as compared to *t*-MTUCB alone, n.s. = not significant. All assays were performed using HepG2 cells.

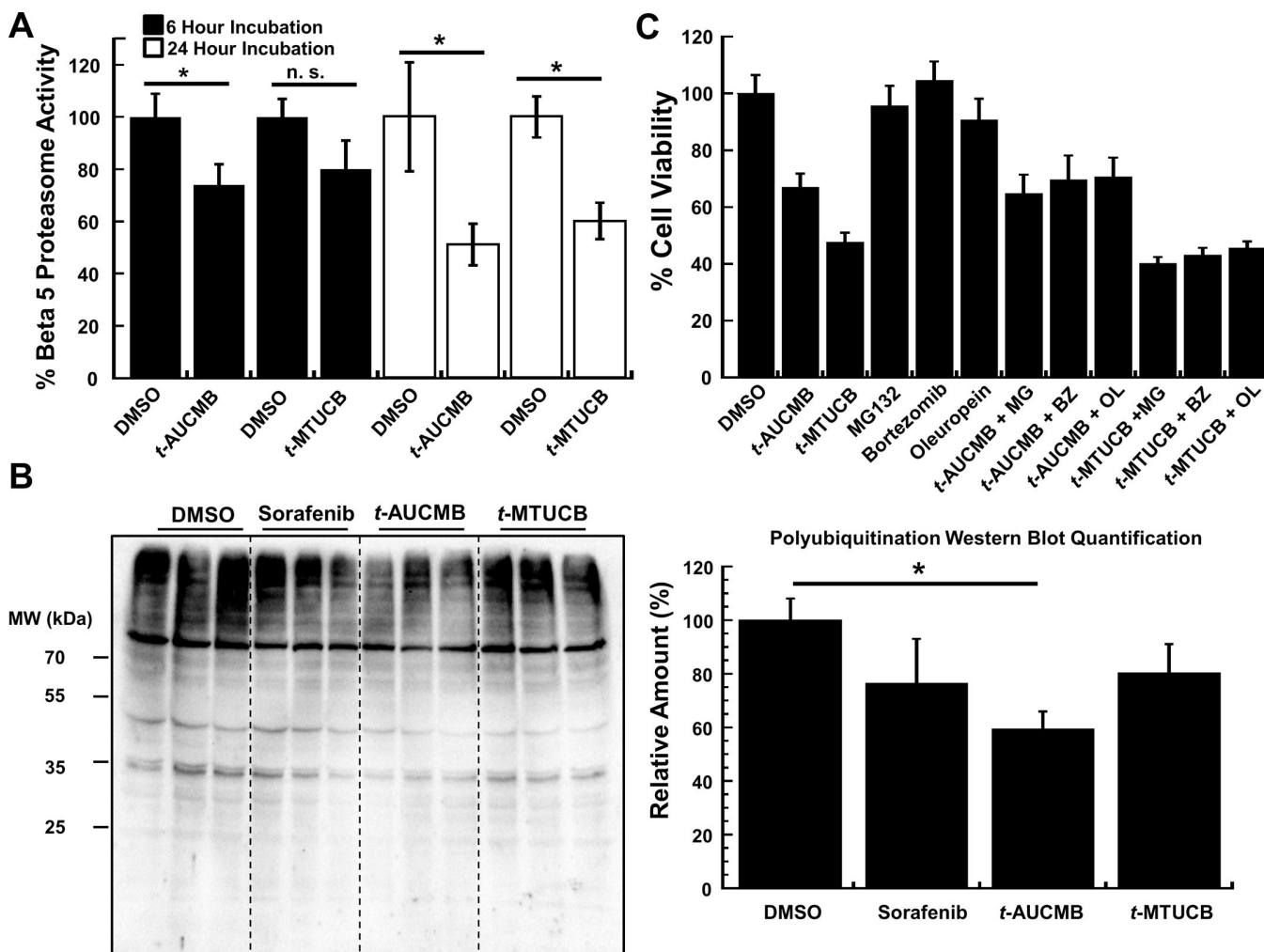
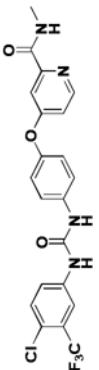
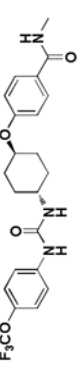
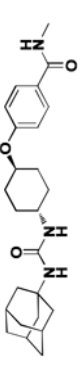


Figure 7. *t*-AUCMB and *t*-MTUCB indirectly inhibit the ubiquitin proteasome system (A) Cellular inhibition of beta 5 proteasome activity after treatment with 30 μ M test compound. **P* value <0.05, n.s. = not significant (B) Polyubiquitination pattern and densitometry quantification after 6 hours exposure with 30 μ M. No increase in ubiquitinated proteins was observed. (C) Cell viability effects upon co-treatment with proteasome inhibitors, bortezomib (BZ) and MG132 (MG), and the proteasome activator, oleuropein (OL), after 6 hours exposure with 30 μ M of sorafenib analogues. Proteasome modulators were tested at 10 μ M. No significant differences were observed. Assays were performed using HepG2 cells. **P* value <0.05 as compared to *t*-AUCMB alone. #*P* value <0.05 as compared to *t*-TMUCB alone.

Table 1

Structures of sorafenib analogues and half-maximum effective concentration (EC_{50}) values (μM) on the cell viability of various cancer cell lines.

Compound Name	Structures	EC_{50} (μM) ^a					
		Liver ^b		Kidney	Prostate	Breast	
		HepG2	Huh-7	ACHN	PC-3	T47D	SKBR3
Sorafenib		4.5 ± 0.7	4.2 ± 0.5	4.0 ± 0.5	5.5 ± 0.8	3.0 ± 0.5	6.5 ± 0.5
<i>t</i> -MTUCB		7.0 ± 0.5	5.5 ± 1.0	6.5 ± 0.7	10 ± 1.0	25 ± 4.0	25 ± 5.0
<i>t</i> -AUCMB		6.0 ± 1.0	7.0 ± 0.5	4.5 ± 0.8	2.5 ± 0.5	4.5 ± 0.5	7.5 ± 0.5

^a Cell viability was determined using MTT assay after 72 hour treatment for sorafenib and 24 hours treatment for the analogues. Assays were performed in 96-well plates with 10,000 cells/well. Data presented as mean ± standard deviation.

^b Data from previous published work [2].